AFGL-TR-78-0058
AIR FORCE SURVEYS IN GEOPHYSICS, NO. 384

Measurements of Atmospheric Density at Kwajalein Atoll, 18 May 1977

C. R. PHILBRICK
A. C. FAIRE
D. H. FRYKLUND

30 January 1978
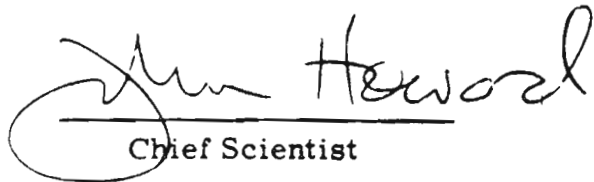
This report has been reviewed by the ESD Information Office (OI) and is releasable to the National Technical Information Service (NTIS).

This technical report has been reviewed and is approved for publication.

FOR THE COMMANDER

Chief Scientist

Qualified requestors may obtain additional copies from the Defense Documentation Center. All others should apply to the National Technical Information Service.

REPORT DOCUMENTATION PAGE	READ INSTRUCTIONS BEFORE COMPLETING FORM

1. REPORT NUMBER	2. GOVT ACCESSION NO.	3. RECIPIENT'S CATALOG NUMBER
AFGL-TR-78-0058		

4. TITLE (and Subtitle)	5. TYPE OF REPORT & PERIOD COVERED
MEASUREMENTS OF ATMOSPHERIC DENSITY AT KWAJALEIN ATOLL, 18 MAY 1977	Scientific. Interim.
	6. PERFORMING ORG. REPORT NUMBER AFSG No. 384

7. AUTHOR(s)	8. CONTRACT OR GRANT NUMBER(s)
C. R. Philbrick, A. C. Faire and D. H. Fryklund*	

9. PERFORMING ORGANIZATION NAME AND ADDRESS	10. PROGRAM ELEMENT, PROJECT, TASK AREA & WORK UNIT NUMBERS
Air Force Geophysics Laboratory Hanscom AFB Massachusetts 01731	627A5501

11. CONTROLLING OFFICE NAME AND ADDRESS	12. REPORT DATE
Air Force Geophysics Laboratory Hanscom AFB Massachusetts 01731	30 January 1978
	13. NUMBER OF PAGES 113

14. MONITORING AGENCY NAME & ADDRESS(if different from Controlling Office)	15. SECURITY CLASS. (of this report)
	Unclassified
	15a. DECLASSIFICATION/DOWNGRADING SCHEDULE

16. DISTRIBUTION STATEMENT (of this Report)

Approved for public release; distribution unlimited.

17. DISTRIBUTION STATEMENT (of the abstract entered in Block 20, if different from Report)

18. SUPPLEMENTARY NOTES

*Accumetrics Corp., Cambridge, MA.

19. KEY WORDS (Continue on reverse side if necessary and identify by block number)

Upper atmosphere density
Upper atmosphere temperature
Accelerometer
Drag acceleration
Atmospheric variability
Mesosphere and thermosphere

20. ABSTRACT (Continue on reverse side if necessary and identify by block number)

A triaxial piezoelectric accelerometer has been used to measure atmospheric drag acceleration on a falling sphere to determined atmospheric density. The technique allows determination of atmospheric density between 50 and 150 km, with an accuracy better than 5 percent and with an altitude resolution of about 200 m. Comparisons have been made with radar determined drag acceleration measurements, with rocketsonde measurements, and with passive Robin sphere density measurements during the same period.

DD FORM 1473 1 JAN 73   EDITION OF 1 NOV 65 IS OBSOLETE

Preface

1

2

3.

4.

R

A

A:

A}

AF

Contents

Illustrations

Measurements of Atmospheric Density at Kwajalein Atoll, 18 May 1977

1. INTRODUCTION

In order to determine the influence of atmospheric parameters on the dynamics of reentry vehicles, a density measurements program was formulated and supported by the SAMSO/ABRES program office. Several of the current and future advanced ballistic tests, require in situ measurements of atmospheric properties in order to properly evaluate the mission performance. The density measuring techniques presently available which have been included in the programs of the ABRES office include radiosondes, rocketsondes, Robin spheres, and accelerometer instrumented spheres. These measuring techniques have been employed to measure the atmospheric density, temperature, and winds near the reentry region around Kwajalein Atoll in the Pacific Ocean where the tests of reentry effects on ICBM systems are frequently evaluated.

The radiosonde measurements provide high accuracy data up to about 33 km (110 k ft). A sufficient number of these measurements have been performed to determine that the errors associated with the radiosondes, which include a hypsometer, are ~0.28 percent (RMS) at 18 km (50 k ft) and 0.42 percent (RMS) at 30 km (100 k ft) (Cole and Kantor[1]). For altitudes above 30 km, the rocketsonde system provides measurements to about 55 km during sunlit periods and about 65 km at night. The

1. Cole, A.E., and Kantor, A.J. (1977) Private communications.

density profile is determined by a normalization to radiosonde data near 30 km. The RMS errors associated with densities derived from the rocketsonde instrument measurements, increase from about 0.4 percent at 30 km to 1.8 percent at 60 km (Cole and Kantor[1]). Above 60 km, the Robin sphere system provides data with an accuracy of about ±5 percent to 80 km and about ±10 percent near 90 km. Most Robin sphere flights provide data to 35 km overlapping the rocketsonde, but differences have been observed and are attributed to poor knowledge of the drag conditions during this subsonic portion of the flight (Kennedy and Hackerson[2]). Since the Robin sphere is a passive system it is totally dependent upon the tracking radar for its data, and is thus subject to the errors of the particular radar system used. Smoothing of the tracking data over several kilometers is necessary to remove the random errors. A significant effort has been made to attempt to improve the accuracy of Robin data by making use of the sophisticated radar systems available at the KREMS facility at Kwajalein Atoll (Martin and Azzarelli,[3] and Hanrahan[4]). These studies have shown that below 80 km, the density errors due to radar tracking data and smoothing are probably less than 3 percent when using the doppler velocity data of the KREMS radars (Hanrahan[4]). Allowing for other error sources should result in an overall density accuracy of about ±5 percent for altitudes below 80 km. The accelerometer instrumented sphere, which is the main subject covered in this report, provides the capability of making measurements from about 50 km to above 150 km with an accuracy of better than ±5 percent over the altitude range. The accelerometer measurements provide better altitude resolution because they are not subject to the difficulties encountered in smoothing radar data.

A new data reduction program has been prepared for the accelerometer sphere over the past few months. The new analysis approach provides accelerometer results with significantly less smoothing and greater accuracy than data previously analyzed. The sinewave type output of the spin plane sensors is fitted to determine a unique acceleration value each half spin cycle. Since there are two spin plane sensors, unique data points are available each 0.05 sec which would allow atmospheric structure with scales of about 150 m to be resolved.

The results discussed in this report are those obtained from measurements made on 18 May 1977 at Kwajalein Missile Range in support of the TDV-1 mission for the SAMSO/ABRES Program Office. Table 1 provides a list of the

2. Kennedy, B.W., and Hackerson, L.D. (1977) Analysis of Meteorological Data at Kwajalein Missile Range for WTR Mission 2333, ASL.

3. Martin, L., and Azzarelli, T. (1977) Wind and Density Measurements on Four ROBIN Spheres, XONICS DCD391.

4. Hanrahan, T. (1977) Evaluation of Doppler Modulation and Angle Error Effects on ROBIN Sphere Atmospheric Density Estimates, XONICS DCD426.

Table 1. Atmospheric Measurements Performed at KMR on 18 May 1977 in Support of TDV-1

Time (GMT)	Mission ID	Sensor
0508	R 12	Rawinsonde (Roi Namur)
0508	K 174	Rawinsonde (Kwajalein)
0655	2024	Rocketsonde
0726	2025	Robin Sphere
0920	2026	Robin Sphere
0940	R 13	Rawinsonde
0940	K 174	Rawinsonde
1037	2027	Robin Sphere
1154	WTR 2333	TDV-1
1237	2028	Robin Sphere
1320	2029	Robin Sphere
1343	0978	AFGL Accelerometer Sphere
1402	2030	Rocketsonde
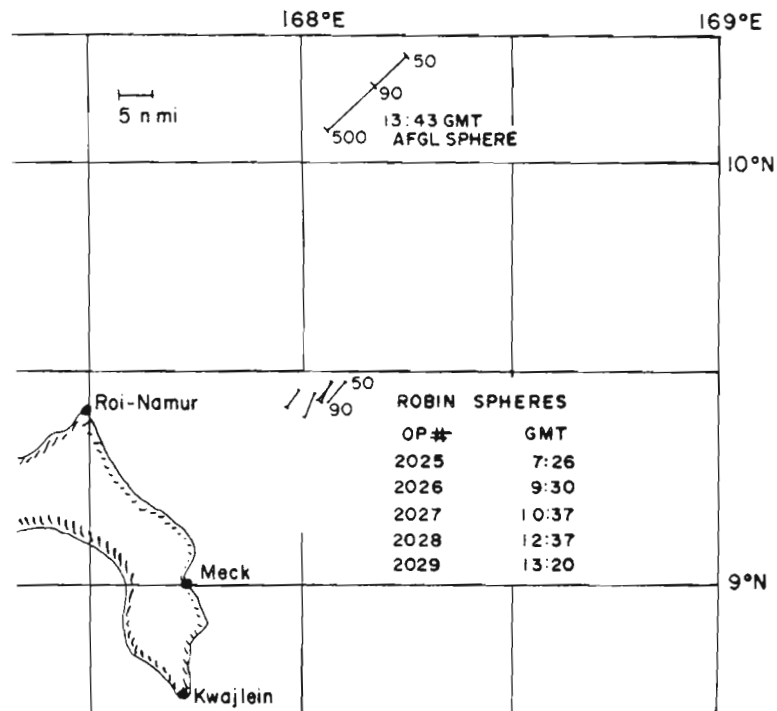
Figure 1. The Region Around Kwajalein Atoll With the Ground Tracts of Where Measurements Were Made. Altitudes on tracts are shown in k ft for the Robin spheres and AFGL sphere

it
a
.
ut

<ing
em
e-
ove
ail-

ie
ig
.
for
nain
;
ver

iing

here
re-
ly
ie

.

ion

)ata

'our

'ects

measurements made during the program. Figure 1 shows the locations around Kwajalein Atoll where the measurements were made.

2. EXPERIMENT DESCRIPTION

An accelerometer capable of accurately measuring atmospheric drag acceleration between 10^{-1} and 10^{-7}, has been developed to provide measurements of atmospheric density from 50 to 150 km. The instrument with its associated electronics, PCM encoder, telemetry transmitter, radar beacon, and batteries have been packaged into a 25-cm diameter sphere.

2.1 Piezoelectric Accelerometer

The accelerometer is a triaxial piezoelectric sensor with the center of gravity of the three proof masses located near the center of the sphere. The piezoelectric crystals used for each axis provide a highly linear output voltage, as a function of the strain produced in the crystal under the force produced by the acceleration of the proof mass.

In Figure 2, an individual sensor element is represented schematically. The sensor is a cantilever beam made in a bimorph construction. The ceramic element used is multicrystalline lead zirconate-lead titanate. This element was selected because of its high sensitivity, good mechanical strength, high internal capacitance, good chemical stability, and good thermal stability. An applied force produces a corresponding deflection that strains the crystal resulting in voltage signal proportional to the applied force. The sensor elements used result in typical outputs of about 70 volts/g. A photograph of the instrument used for rocketborne sphere measurements is shown in Figure 3. Because the high acceleration forces from handling and launching the sphere could fracture the ceramic, the proof masses are held clamped until after the sphere is released from the payload. In order to determine the total drag acceleration at any particular time on the sphere, three orthogonal axis of measurements are desired. The configuration of concentric masses allows the center of mass of each proof mass to be located near the center of gravity of the sphere. During assembly and balancing, the first and second moments of inertia of the instrument are adjusted so that the spinning sphere will be gyroscopically stable and that the precession frequency will be well removed from the measurement, or spin frequency. The sphere is flown with the sensitive direction of the z-axis along the rocket longitudinal axis. The final spin rate is typically in the range between 5 and 6 Hz and precession frequency about 1 Hz. The sphere is released with a mechanism designed to impart a large separation velocity from the payload, and to produce minimum forces that would result in precessional motions.

EDGE VIEW OF PIEZOELECTRIC BIMORPH

ELECTRICAL CONTACT

CERAMIC PLATE
BRASS SHIM
CERAMIC PLATE

PROOF MASS

EACH SIDE OF CERAMIC PLATE
IS SILVER COATED - POLARIZATION
DIRECTION OF CERAMIC SHOWN BY
ARROW
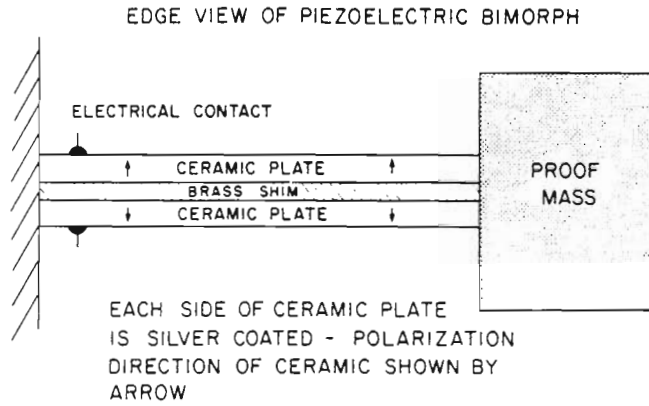
Figure 2. A Schematic Representation of the Sensor
Construction Indicating the Orientation of the Polari-
zation Field of the Piezoelectric Ceramic

DIMPLE MOTORS

CAGING JAWS

Y-AXIS BIMORPH

X-AXIS BIMORPH

ACCELEROMETER MECHANICAL COMPONENTS

Z-AXIS BIMORPH

SEISMIC MASSES
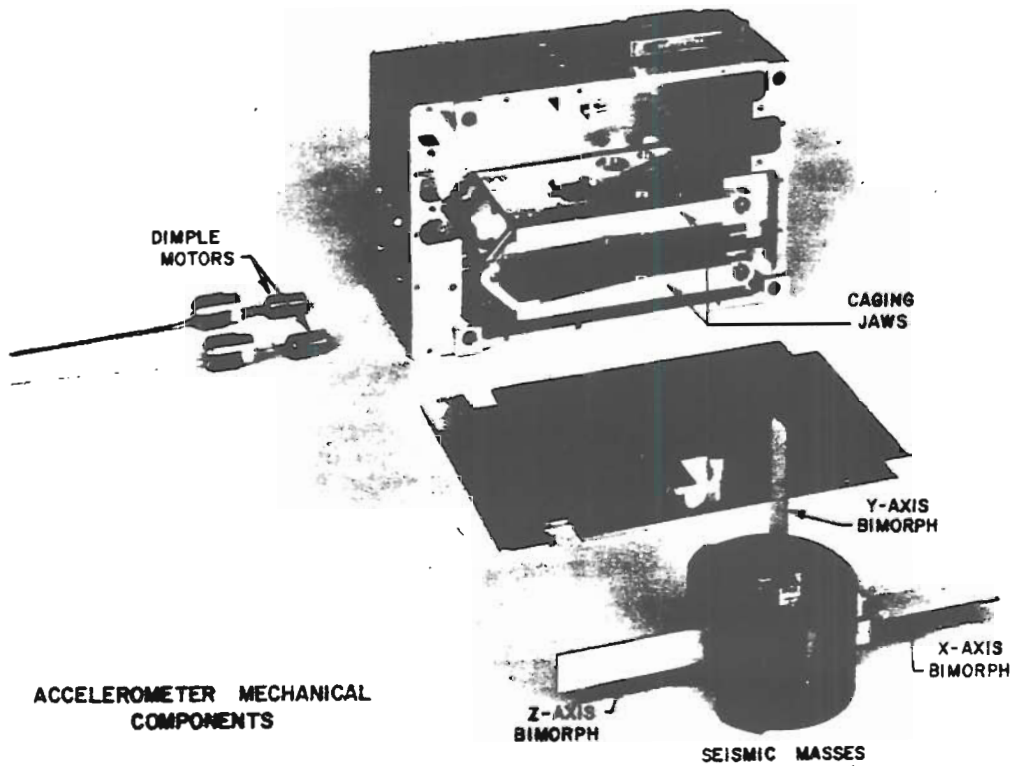
Figure 3. A Photograph of the Sensor Housing, Which is Machined Out of Solid
Stock for Rigidity, Showing the Caging Jaws and the Bimorph Elements With Their
Proof Masses

13

2.2 Experiment Measurements

The atmospheric drag acceleration is colinear with and oppositely directed from the velocity. Figure 4 shows the angles defined for the sphere data analysis. After the sphere is released, its spin axis tends to stay fixed in inertial space. The precession motion typically results in a cone with a half-angle of about one degree superimposed on the mean spin axis direction. The spin stability should not allow the misalignment of center of mass and center of pressure, to cause a change in the mean spin axis direction to accumulate to an angle greater than $1/2^{\circ}$ over the usable altitude range. The angle, α, between the vertical and the spin axis can be determined by two independent techniques and once known, it leads directly to independent measurements of drag acceleration from each of the sensor outputs. The relationships are:

$$\beta + \gamma - \alpha = 180^{\circ} \quad ,$$

$$a_D = \frac{a_x}{\sin \gamma} \quad ,$$

$$a_D = \frac{a_y}{\sin \gamma} \quad ,$$

$$a_D = \frac{a_z}{\cos \gamma} \quad ,$$

where

α is the angle between the spin axis and vertical,

β is the angle between the velocity vector and vertical,

γ is the angle between the drag acceleration vector and the spin axis,

a_z is the acceleration component along the planned spin axis which is smoothly and slowly changing during a flight,

a_x and a_y are the peak amplitudes of sine curves, produced each spin period by the component accelerations in the spin plane.

One of the ways of determining the value of α is to use the a_x or a_y component together with a_z, calculating γ from,

$$\gamma = \tan^{-1} \frac{a_x}{a_z} = \tan^{-1} \frac{a_y}{a_z}$$

14

$$\vec{a}_D \quad \alpha \quad \gamma \quad \beta \quad a_z \quad a_x \quad a_y \quad \vec{\nu}$$

$$\alpha = \beta + \gamma - 180°$$
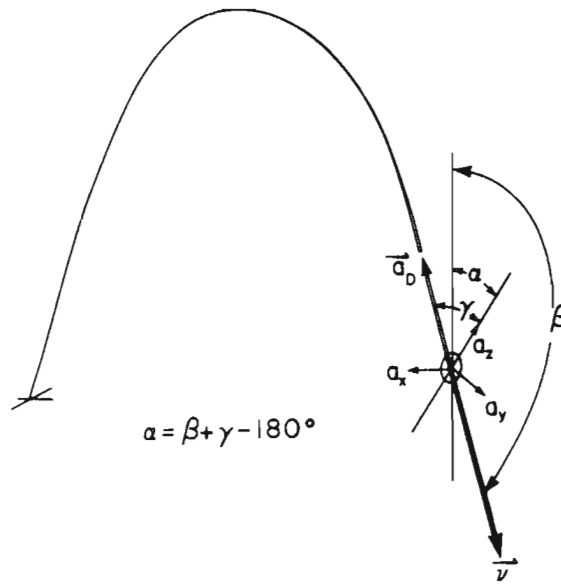
Figure 4. Representation of the Angles Used
in the Analysis of the Sphere Data

with β known from the trajectory velocity components. Second, under the assump-
tion that the spin vector stays fixed in space, the value of α can be determined as
that value necessary to have reasonable agreement between a_D values on upleg,
with those on downleg using a_x or a_y measurements. Note from Figure 4 that on
upleg the angle between a_D and a_y is near $90°$. This fact leads to a very sensitive
dependence of upleg a_y values on the chosen α. This point will be illustrated later.

Each axis output voltage is sensed by a series of four amplifiers which have
gain differences of about a factor of 20. The amplifiers have notch filters to
strongly attenuate the signals at the precession frequency. This minimizes the
effects such as precessional motion of the sphere, particularly at the higher gain
levels. Typically, the spin frequency is 5 to 6 Hz and the nutation frequency about

0.9 Hz with a nutation angle of about 1 to $2°$, which is measured by an accelerom-
eter removed from the center of the sphere. The amplifiers are calibrated at about

20 different frequencies to determine the appropriate transfer function. In Fig-
ure 5 the amplifier calibration curves for the y-axis show the notch filter centered

at 0.9 Hz.

The precession frequency determined from the flight data was 0.9052 ± 0.0001 Hz
compared to the calculated value of 0.8874 Hz, that would be expected from labora-
tory measurements of the finally adjusted moments of inertia. The precession an-
gular velocity, λ, is related to the spin angular velocity, ω, by the relationship,
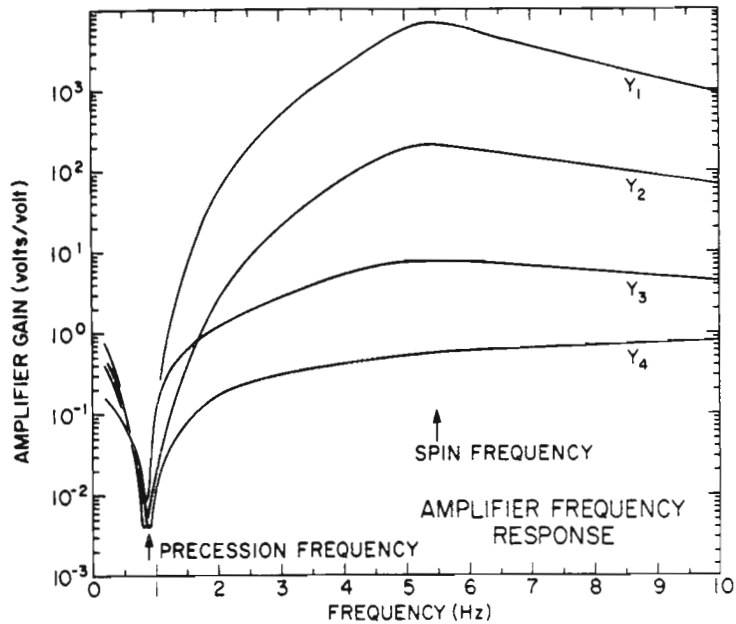
Figure 5. Amplifier Gain Curves Plotted as a Function of Frequency From the Y-axis Calibration Data. The effect of the twin-T filter at the precession frequency is shown

$$\lambda = \omega \left(\frac{I_z}{I_{xy}} - 1 \right) \quad ,$$

where I_z and I_{xy} and the moments of inertia about the spin axis and any axis in the x-y plane, respectively. An error of 0.27 percent in the measurement of the sphere moment of inertia ratio during the laboratory calibration accounts for the difference between the measured and calculated precession frequencies.

The free nutation or precession acceleration is measured by a low sensitivity accelerometer, located about 10 cm from the center of the sphere with its sensitive axis parallel to the z axis. The precession acceleration measurement can be used to determine the cone angle of the z axis of the sphere. An Euler angle analysis of the motion of the sphere yields the relation, in small angle approximation,

$$a_p = r \, \theta \, (\omega^2 - \lambda^2) \quad ,$$

where a_p is the precession acceleration at the radial distance r from the center of the sphere and θ is the cone angle. Analysis of the flight results in the vicinity of 80 km on upleg and downleg, shows that the cone angle was 1.84° on upleg and

16

0.97° on downleg. The decrease in coning angle between the up and downleg is caused by damping due to flexing of mechanical parts in the sphere. The cone angle observed on downleg produces an acceleration superimposed on the drag acceleration of ±1 to 1.5 percent.

Once the drag acceleration, a_D, has been determined, the atmospheric density, ρ, can be determined from the drag force,

$$F = \frac{1}{2} \rho v^2 C_D A = m a_D$$

$$\rho = \frac{2 a_D m}{v^2 C_D A} \quad .$$

The drag coefficient, C_D, can be determined from experimental results in the range of Reynolds numbers between 20 and 10^5, and for Mach numbers between 0.1 and 6 (Bailey and Hiatt[5]) and from theoretical studies in the free molecular flow region (Schaaf and Chambre[6]). In the transitional flow region which corresponds to altitudes between 90 and 110 km, a model solution (Rose[7]) compatible to smooth transition between the continuum and free molecular cases is used. At lower altitudes the drag coefficient can be conveniently expressed in terms of Reynolds number and Mach number. At high altitudes the important parameters are the speed ratio and Knudsen number. But, in both cases, the atmospheric temperature is needed. A convenient table for determination of drag coefficient (Corbin[8]), based on the models mentioned, is used in this analysis. Thus, for the first solution a model atmosphere is used to provide the parameters to define the drag coefficient. The mass density is calculated and this used to calculate the temperature under the assumption of hydrostatic equilibrium. This calculated temperature is then used to recalculate the drag coefficient. When final density values are obtained, these results can be used to calculate molecular scale temperature which is converted to gas kinetic temperature using model values of mean molecular weight.

5. Bailey, A.B., and Hiatt, J. (1972) AIAA 10:1436.
6. Schaaf, S.A., and Chambre, P.L. (1958) Fundamentals of Gas Dynamics, 687.
7. Rose, M.H. (1964) Phys. Fluids I:1262.
8. Corbin, V.L. (1975) Private communication of unpublished study, Drag Coefficients from Free Molecular Flow to Continuum Flow for Mach Numbers 1.5 to 6.0.

17

2.3 Atmospheric Model

The atmospheric model used for all of the comparisons shown in this report is the U. S. Standard Atmospheric Supplements 1966, 15°N Annual (USSAS[9]) which is the source for the Kwajalein Standard Atmosphere (Salah[10]) and is identical with it. Above 120 km, the USSAS 1966 summer model with an exospheric temperature of 800°K has been chosen for use. This choice provides a realistic comparison with a continuous value and slope through the 120 km level. The mean molecular weight is taken to be 28.96 up to 80 km, from 80 to 120 km the values of USSAS 1966 (Table 2.3) are used, and above 120 km the model values consistent with the summer $T_{ex} = 800^{\circ}$K model are used.

2.4 Calibration Procedures

Each sensor with its proof mass is calibrated by applying a sinusoidal motion to the support mounting, measuring the distance traveled at a fixed frequency and thus determines the acceleration of the mass. In Figure 6, a schematic representation of the calibration setup is shown. The distance traveled is measured with a telescope reticle which is calibrated with precision gauge blocks.
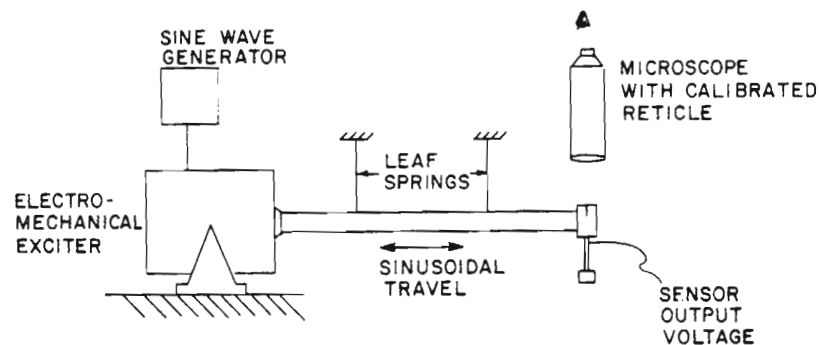
Figure 6. Schematic Diagram of the Test and Calibration Arrangement Indicating the Measurement of the Displacement With a Microscope to Determine the Input Acceleration

9. USSAS (1966) U. S. Standard Atmospheric Supplements, 1966, U. S. Government Printing Office, Washington, D. C.

10. Salah, J. E. (1967) Kwajalein Standard Atmosphere, MIT Lincoln Laboratory Technical, Note 1967-14.

The applied motion during calibration is,

$$x = X \sin \omega t \quad,$$

from which the acceleration is given by,

$$\ddot{x} = -\omega^2 X \sin \omega t \quad,$$

and has a peak acceleration of,

$$\ddot{x} = \omega^2 X \quad.$$

The peak acceleration can be easily determined from the measurement of the frequency and the maximum displacement. The natural frequency is measured by shock-exciting the transducer while it is vertically suspended on the calibration system. The equation of force for this system includes a pendulum-like restoring force and can be written,

$$m\ddot{x} = -kx - \frac{mgx}{\ell} \quad,$$

or

$$\ddot{x} + \left(\frac{k}{m} + \frac{g}{\ell} \right) x = 0 \quad,$$

where the natural frequency is seen to be,

$$f_n = \frac{\omega}{2\pi} = \frac{1}{2\pi} \left(\frac{k}{m} + \frac{g}{\ell} \right)^{1/2} \quad.$$

The observed frequency of free vibration when the system is shock-excited in the laboratory will thus be higher than the natural frequency, $f_n = 1/2\pi \sqrt{k/m}$ experienced at zero-g. The typical natural frequencies of these sensors are in the range of 12 to 14 Hz and for bimorph lengths of 5 to 6 cm, frequency differences of about 1.5 percent would be expected. In Table 2, the observed frequencies, expected natural frequencies, and calibration values at test frequencies are listed.

The sensor is used to make measurements under a case of forced undamped oscillations. The frequency used in these calibrations is near 3 Hz. The crystal

Table 2. Calibration Data for the Accelerometer (AC-6) Flown 18 May 1977

Axis	f(test, free oscillation) (Hz)	f_n(test) (Hz)	f(test) (Hz)	Output(test) (Volts/g)	Output(f=0) (Volts/g)
X	12.0	11.82	3.05	69.94	65.29
Y	14.4	14.23	3.0625	67.12	64.10
Z	13.7	13.53	3.06	67.72	64.26

calibration is then corrected to zero frequency by use of the standard amplification factor equation (c.f. Thomson[11] or Van Name[12])

$$\frac{A}{A_o} = \frac{1}{\left\{ 1 - \left(\frac{\omega}{\omega_n}\right)^2 \right\}^2 + \left(2\zeta \frac{\omega}{\omega_n}\right)^2} \quad ,$$

where ζ is the damping factor. The damping factor can be easily determined by looking at the logarithmic decrement, δ, when the crystal is placed in free vibration, $\delta = 1/n(\ln)(x_o/x_n)$. For small damping factors, $\zeta \cong \delta/2\pi$, and for typical sensors of the type used here, the damping factors range between 5×10^{-3} to 8×10^{-3}. Thus, $(2\zeta \omega/\omega_n)^2 \cong 0$ and the amplification factor reduces to the form,

$$\frac{A}{A_o} = \left| \frac{1}{1 - (\omega/\omega_n)^2} \right| \quad ,$$

and can be used to calculate the amplification at any forcing function frequency. Figure 7 shows amplification factor plotted as a function of the ratio of angular velocity or frequency ratio to its natural value when in free oscillation.

In the flight data, the free vibration frequency can be determined immediately after the masses are uncaged. Table 3 shows the values of frequency observed in flight with amplification factors and flight sensitivities. The natural frequency is not the same as that observed after uncaged, because the spin produces an additional force due to centripetal acceleration unless the proof masses are located exactly at the center of gravity. The force equation is,

11. Thomson, W.T. (1948) Mechanical Vibrations.

12. VanName, F.W., Jr. (1958) Analytical Mechanics.

20

ion
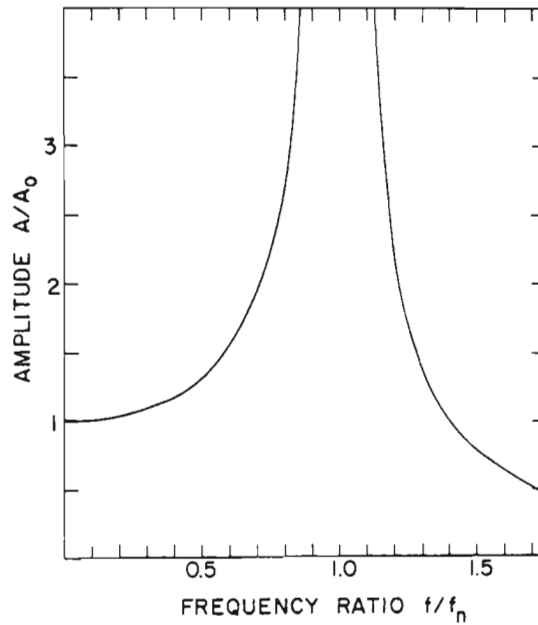
Figure 7. The Amplification Factor of a
Forced Undumped Oscillator is Plotted as a
Function of the Ratio of the Forcing Fre-
quency to the Natural Frequency of the
Oscillator

y

·a-

n,

Table 3. Free Oscillation Frequency and Flight Sensitivities for
Accelerometer AC-6

Axis	f(flight free oscillation) (Hz)	A/A_o	f(spin) (Hz)	f_n(flight)	Flight Sensitivity (Volts/g)
X	10.72	1.383	5.644	12.11	90.31
Y	11.88	1.291	5.644	13.15	82.67
Z	---	1.0	---	---	64.26

ly

ed in

:y is

di-

ed

21

$$m\ddot{x} = -kx + m\,x\,\omega_3^2 \quad,$$

or

$$\ddot{x} = -\left(\frac{k}{m} - \omega_s^2\right)x \quad,$$

where the observed angular velocity, $\omega = (k/m - \omega_s^2)^{1/2}$, which can be rewritten, $f_n^2 = f_{obs}^2 + f_s^2$, and ω_s and f_s represent the spin angular velocity and frequency, respectively. The natural frequencies calculated for the flight case are different than those for the test case. The difference is probably due to the rigidity of the mounting box compared to the test stand. The values used to determine the flight sensitivity are those determined after the accelerometer is uncaged in flight.

The ratio of acceleration measurements from the x and y axes are shown in Table 4. The fact that the variation is much larger than the standard deviation of the measurements is probably due to the calibration accuracy of the individual amplifier gains. The sine function voltage generator used in the calibration of these amplifiers was later found to exhibit intermittant second harmonic distortion which contributed at least some errors to the calibration and is the main source of error for the results presented in this report. Analysis of the calibration data and recent tests with the piece of equipment, have led to the conclusion that errors up to 5 percent could have been introduced. The difference between the a_{y1} and a_{x1} ranges is probably due to this error source. The agreement of the flight results with the rocketsonde data at low altitudes, leads to the conclusion that the results are probably less than the 5 percent mentioned; however, this factor must be considered in evaluating the absolute errors of this experiment.

Table 4. Ratio of the Measurements of X-axis and Y-axis Acceleration With Standard Deviation for 25 Data Points in the Upper Portion of Each Range

a_{y4}/a_{x4}	$1.016 \pm .005$
a_{y3}/a_{x3}	$0.987 \pm .006$
a_{y2}/a_{x2}	$0.987 \pm .004$
a_{y1}/a_{x1}	$0.967 \pm .004$

22

2.5 Analysis Procedures

The outputs from the accelerometer amplifiers are encoded into 8 bit PCM words for each of the four amplifier ranges of the three axes. The 16 PCM words, making one frame of data, are encoded and transmitted at 100 values per second. At typical spin frequencies of 5 to 6 Hz, there are about 20 values making up the measurements of each spin cycle (see Figure 8). The spin frequency for this sphere was 5.644 Hz. The PCM output counts are fitted to a sine curve for 20 sequential values, approximately one spin, and then the first 10 values dropped, 10 new sequential values added, and a new fit determined. This procedure continues and provides the amplitude of each fit as a fractional count of the PCM data, with values between 0 and ±127 counts. Any bias in the spin axis output is thus removed by the fit. The accuracy of each amplitude determined is approximately $\pm 1/\sqrt{20}$ divided by the number of counts. At saturation of one amplifier range, the next less sensitive range typically reads 5 to 7 counts. Thus at the bottom of a range, each amplitude is accurate to about ±4 percent and at the top of the range ±0.2 percent. The amplitude in counts is converted to voltage using the encoder calibration, approximately 40 millivolts per count. The laboratory determined sensor sensitivities and amplifier gains are then used to calculate the acceleration components. From each acceleration component, a drag acceleration value can be determined after the value of α, the orientation of the sphere axis in space, is found. This procedure was described earlier. The z axis values for this flight have been determined to be in error due to the properties of the filter circuit used for reducing the effects of nutation. The nutation sensor output does, however, provide a measurement of the z component acceleration at low altitudes. The a_z component measured by the nutation sensor was used to correct the z axis acceleration and in turn to calculate the value of α to be 28°. The other technique, described earlier, is to use the upleg measurements as a criteria for determining α. Figure 9 shows the upleg values of a_y for $\alpha = 28^\circ$ and $\alpha = 30^\circ$ compared to the downleg $\alpha = 29^\circ$ values. From this comparison we see that changes of $\pm 1^\circ$ in α result in a change of ±8 percent in the upleg acceleration. The downleg values are changed by less than 2 percent for each 1° change in α, and for this flight the final value of $\alpha = 29^\circ \pm 1^\circ$ has been determined.

2.6 Temperature Determination

The temperature is determined from the density profile under the assumption of hydrostatic equilibrium,

$$dP = - g\rho\, dZ \quad ,$$

ritten,
ency,
lifferent
y of the
he flight
ght.
nown in
-iation of
ridual
:ion of
distortion
source of
on data and
errors up
and a_{x1}
t results
ne results
ıst be con-

23

Figure 8. A Portion of a Strip Chart of the Data Showing the Sine Oscillation of the Sensor Output as the Sphere Spins

24
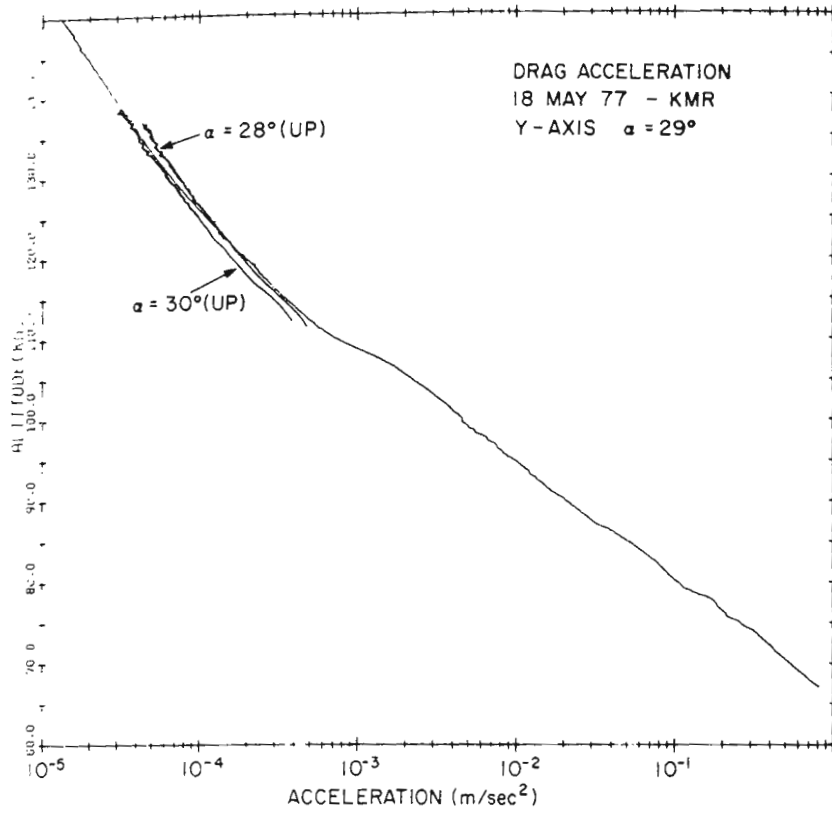
Figure 9. Computer Plot of the Downleg Acceleration Measured by the Y-axis Accelerometer $\alpha = 29^\circ$ With the Upleg Measurements at $\alpha = 28^\circ$ and $\alpha = 30^\circ$ for Comparison

and the ideal gas law,

$$P = \frac{\rho}{M} RT = \frac{\rho}{M_o} RT_M$$

$$T_M = \frac{M_o}{M} T$$

where R is the universal gas constant, M_o is the sea level value of mean molecular weight, and T_M is the molecular scale temperature. These equations can be combined to the form,

$$dP = \frac{R}{M_o} \left\{ T_M d\rho + \rho dT_m \right\}$$

25
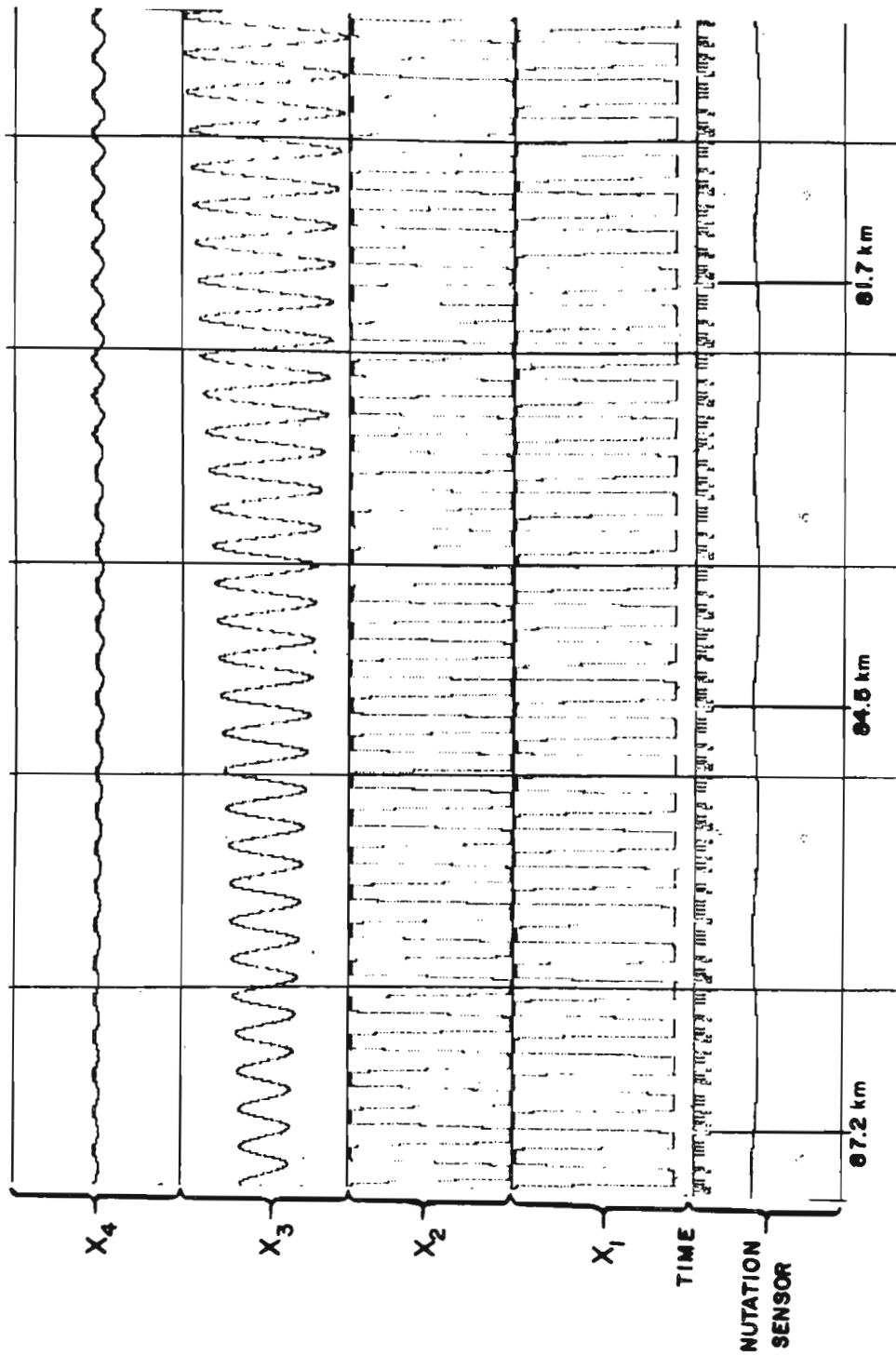
Figure 8. A Portion of a Strip Chart of the Data Showing the Sine Oscillation of the Sensor Output as the Sphere Spins

and yields,

$$T_{M2} = T_{M1} \frac{\rho 1}{\rho 2} - \frac{M_{o}g(z)}{\rho 2\ R} \int_{Z_1}^{Z_2} \rho\ dZ$$

which is integrated along the density profile. The molecular scale temperature obtained is converted to gas kinetic temperature using the model values of mean molecular weight.

The acceleration of gravity used for the calculation is obtained from the relation,

$$g(Z) = \frac{g_\Phi\ R_\Phi^2}{(R_\Phi + Z)^2}\ ,$$

where g_Φ is the sea level acceleration of gravity at latitude Φ and R_Φ is the effective radius of the earth that brings harmony between g_Φ and the vertical gradient of g assuming the earth is represented by the International Ellipsoid (List[13]). The equations for g_Φ and R_Φ are

$$g_\Phi = 9.78035\ (1 + 0.0052885\ \sin^2 \Phi - 0.0000059\ \sin^2 2\Phi)$$

$$R_\Phi = (2g_\Phi)/(3.085462 \times 10^{-6} + 2.27 \times 10^{-9}\ \cos 2\Phi - 2 \times 10^{-12}\ \cos 4\Phi)\ .$$

The values used for this analysis are $g_\Phi = 9.781724$ m/sec^2 and $R_\Phi = 6336.115$ km.

2.7 Payload Configuration

A pictorial representation of the payload is given in Figure 10. The sphere is held in a cradle assembly within a split nosecone. The payload was launched on a Nike-Hydac rocket system (A11.712-1) at 13:43:00.100 on 18 May 1977 from Roi Namur, KMR Operation Number 0978. The payload was despun using a yo-yo weight from $\sim$ 12 Hz to $\sim$ 5.5 Hz at T $\div$ 54.2 sec (59.8 km), the nose tip ejected at T $\div$ 55.4 sec (61.4 km), the sphere released at T + 61.4 sec (70.5 km), and the accelerometer proof masses uncaged at T + 66 sec (77.6 km). The payload provided good data from 110 km on upleg to near 60 km on downleg. S-band telemetry

---

13. List, R.J. (1968) Smithsonian Meteorological Table, 6th Edition, Smithsonian Institution, Washington, D.C.

26

links were carried on the payload for housekeeping information and on the sphere for the PCM data. C-band beacons were included for tracking the payload and sphere. The physical properties for the sphere are given in Table 5.

are
ean

e effec-
dient
'). The

'. 115 km.

ere is
; on a
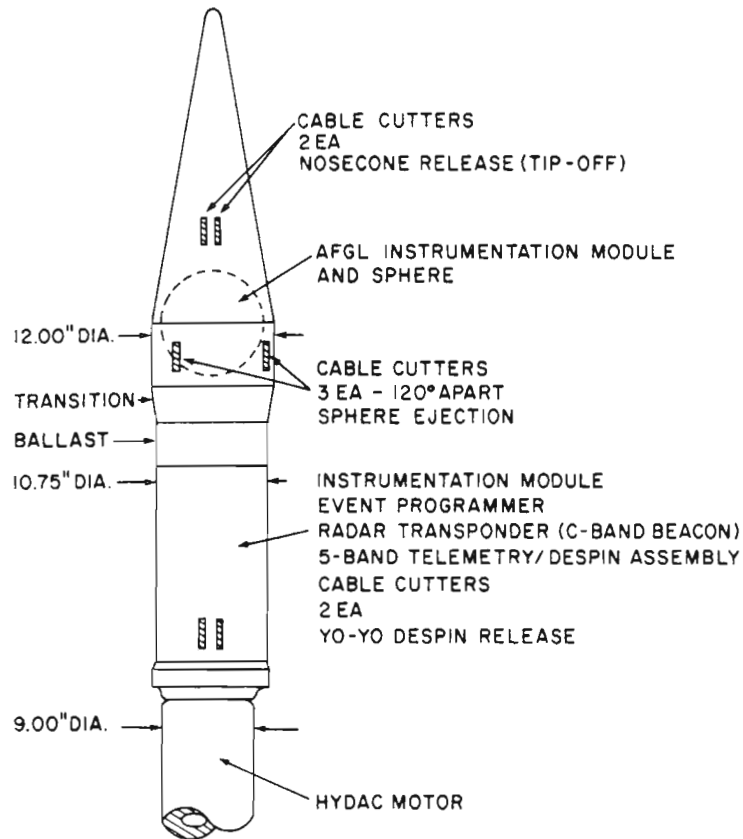Roi
o-yo
jected at
nd the
ad pro-
telemetry

nithsonian

Figure 10. A Diagram of the Sphere Payload Indicates the Location and Configuration of Various Pieces of Equipment

Table 5. Sphere Parameters

Spin axis diameter	- 0.25712 to 0.25723 m
Transverse axis diameter	- 0.25710 to 0.25725 m
Weight	- 9.816 kg
Moment-of-inertia ratio	- 1.157

27

3. EXPERIMENT RESULTS

The mass densities measured between 65 and 150 km on the downleg of the sphere flight from the y-axis accelerometer, are shown in Figure 11. The atmospheric model values are shown for comparison. Because of the difficulty in viewing the results plotted in this way, the ratio to a chosen atmospheric model will be displayed in the following curves. The model chosen for these comparisons, USSAS 1966, was already discussed.

The density ratio shown in Figure 12 displays the individual point by point values of mass density calculated for the y-axis measurements. No smoothing of the data has been done on this or the succeeding two figures. In Figure 12, the data represents the first calculation of density where the model values of temperature are used to calculate the Mach number and Reynolds number used to determine the drag coefficient. In Figure 13, the mass densities have been calculated using the temperature results from the integration of the hydrostatic equation from the density results plotted in Figure 12. This iteration process for arriving at the final results improves the final answers in proportion to their difference from the model. Comparison of Figures 12 and 13 illustrates that when the measured densities are about 20 percent from the model, the correction is ~ 3 percent when the calculated temperature profile is used.

The results presented in Figure 13 represent the final results for the y-axis accelerometer, and Figure 14 shows the final results for the x-axis. Comparison of Figures 13 and 14 shows that both accelerometer axes agree very well in measuring both the magnitude and structure in the atmosphere density. The same large and small scale structures are exhibited in both profiles. The scatter due to the statistical variation of individual points can be observed in these curves. For example, at 123 km in Figure 13 the a_{y1} range is saturated and the a_{y2} range is at a low level. It was commented earlier that at the changeover from one range to another, the more sensitive range data points would be statistically significant to ± 0.2 percent, while the less sensitive range would only be significant to $\sim \pm 4$ percent. It is this statistical scatter that is observed in the vicinity of 120 km. The other range changes that occur in Figure 13 are at 100 km (a_{y2} to a_{y3}) and at 79 km (a_{y3} to a_{y4}). The measurements extend to 62 km for the y-axis. The range changes occur at different altitudes for the x-axis data in Figure 14. The relative profile error is less than 3 percent when data points at the low ends of ranges are lightly smoothed.

A hand-smoothed profile for the measurements below 110 km is shown in Figure 15, along with the results from a rocketsonde measurement about 20 min later. The agreement between the measurements is quite good. The measurements are in agreement within about 2 percent. Table 6 indicates the magnitude of the

the

atmos-

n view-

will be

s, USSAS

oint

hing of

, the

empera-

letermine

d using

om the

t the

rom the

ed densi-

en the

y-axis

nparison

in measur-

e large

e to the

For

nge is at

e to

ant to

4 per-

. The

at 79 km

nge changes

e profile

re lightly

wn in

t 20 min

easurements

de of the
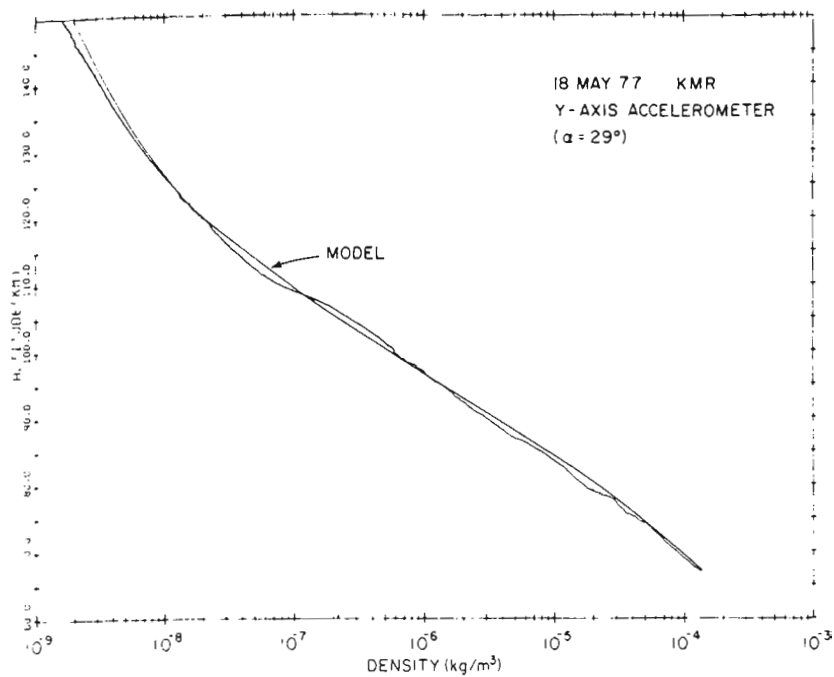
Figure 11. The Mass Density Results Obtained From the Y-axis Accelerometer Shown With the Model Profile
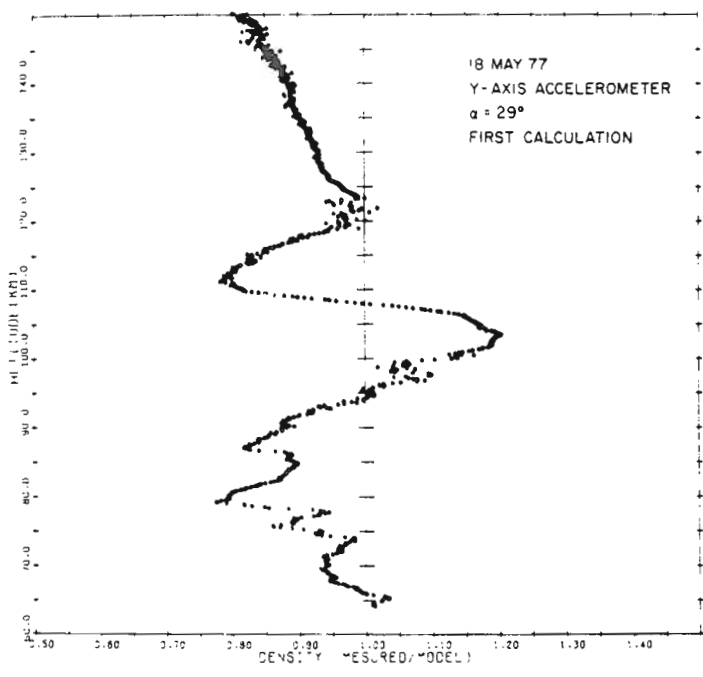
Figure 12. The Y-axis Accelerometer Mass Densities Ratio to Model are Plotted for the First Calculation Which Uses the Model Temperature for Determination of the Drag Coefficient
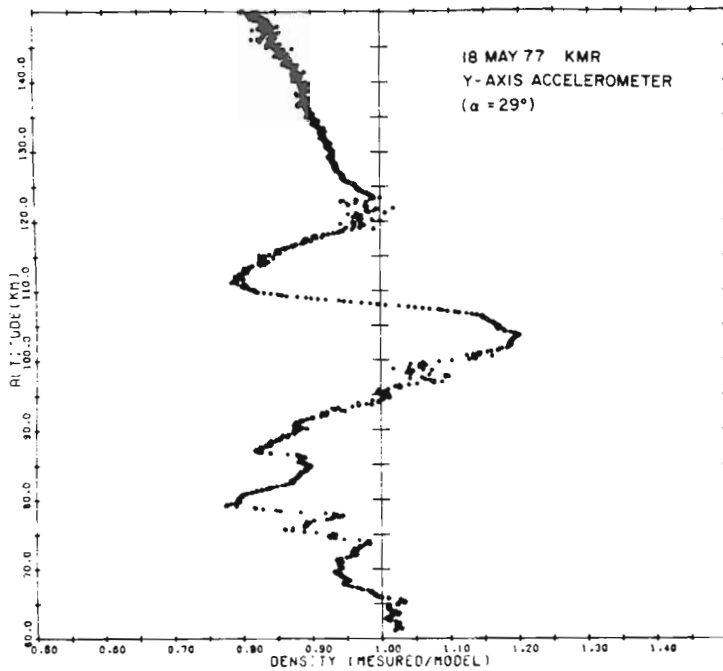
29

Figure 13.   The Final Results of the Y-axis Accelerometer
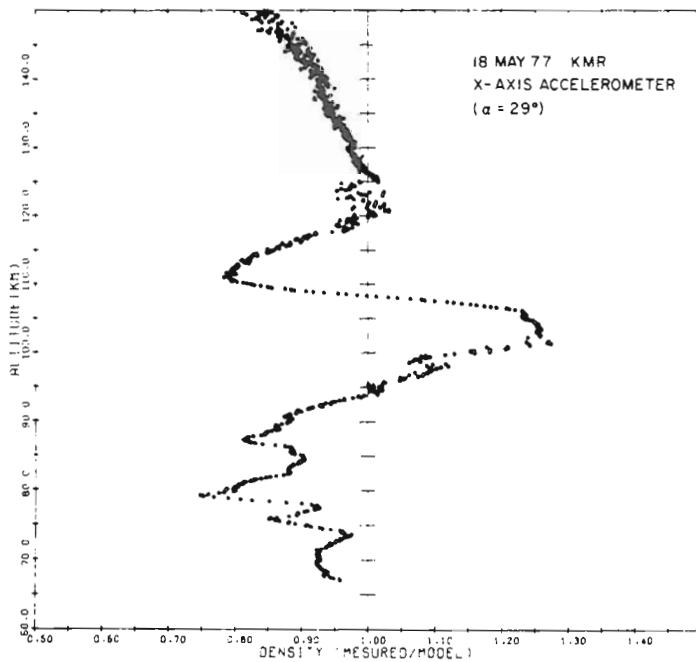Ratio to Model are Plotted

Figure 14.   The Mass Density Results From the X-axis
Accelerometer are Shown as a Ratio to the Model

Alt.
(k

rocketsonde
studies of l;
    The va:
the hydrost:
urements, :
comparison

30
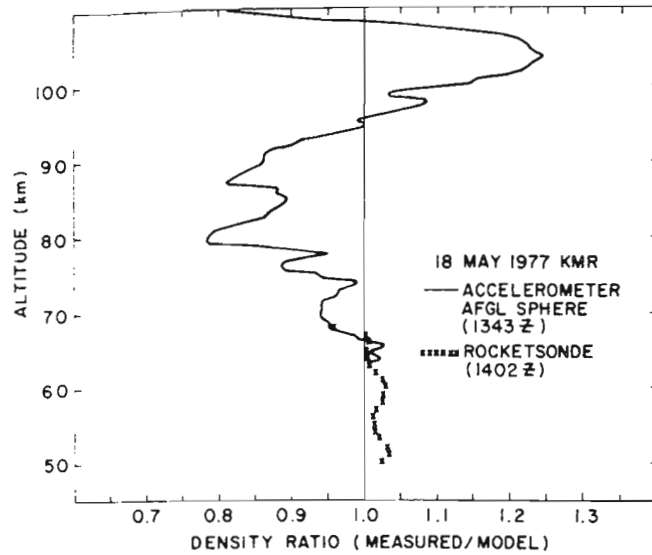
Figure 15. Density Results From an Accelerometer Instrumented Falling Sphere and From a Rocketsonde are Shown as a Ratio to the USSAS, 1966, Model Atmosphere

Table 6. Variability of Rocketsonde Density Measurements From Analysis of Large Data Sets to Determine Observed Variability Relative to Mean Monthly Model and Instrumentation Variability (Cole and Kantor[1])

Altitude (km)	Observed Variability (RMS %)	Instrument Variability (RMS %)	Atmospheric Variability (RMS %)
30	1.6	0.4	1.5
40	2.2	1.0	2.0
50	2.8	1.6	2.3
60	3.9	1.8	3.5

rocketsonde instrument variability which has been determined from statistical studies of large numbers of rocketsonde measurements.

The values for atmospheric temperature determined from the integration of the hydrostatic equation down the density profile determined from the x-axis measurements, are shown in Figure 16. The model temperature profile is shown for comparison. In the regions about 145 km and 120 km, a dash line indicates that the

31
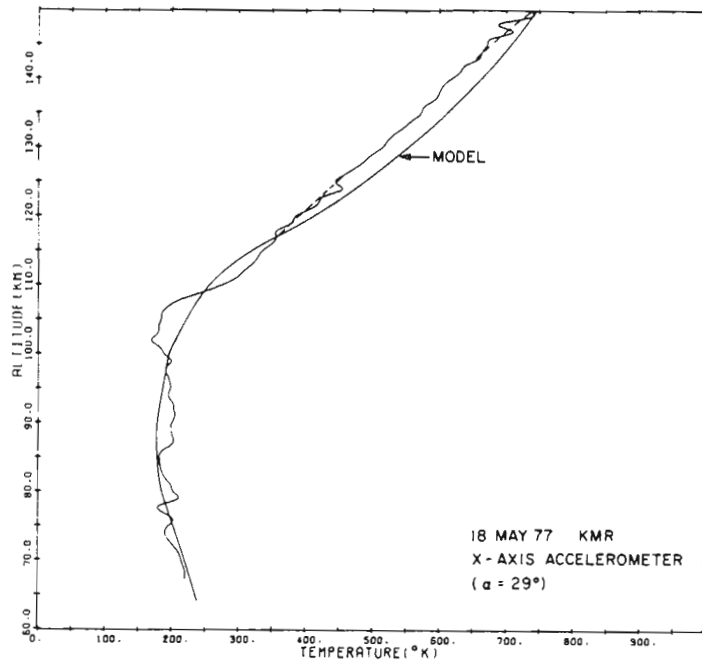
Figure 16. The Temperature Profile Determined From the Density Measurements of the X-axis Accelerometer Compared to the Atmospheric Model. The dash indicates regions of error due to data sampling statistics

structure is not real but an artifact of the statistical accuracy of the points at the lower ends of the output ranges. In Figure 17 the temperature profile determined for the y-axis data is shown. Comparison of the results in Figures 16 and 17 shows excellent agreement in the determined temperatures.

The final results presented here are in general agreement with the preliminary results (Philbrick[14]) prepared in June 1977. The same structural features in the profiles are observed and the magnitudes of the results generally agree within about 5 percent.

The final results for the y and x-axis accelerometers are tabulated in both metric and english units in Appendices A, B, C and D.

14. Philbrick, C.R. (1977) Private communication, Letter Report of Preliminary Data for TDV-1 on 18 May 1977, dated 29 June 1977 from C.R. Philbrick, AFGL, to Capt. Bose, SAMSO/RSSR.

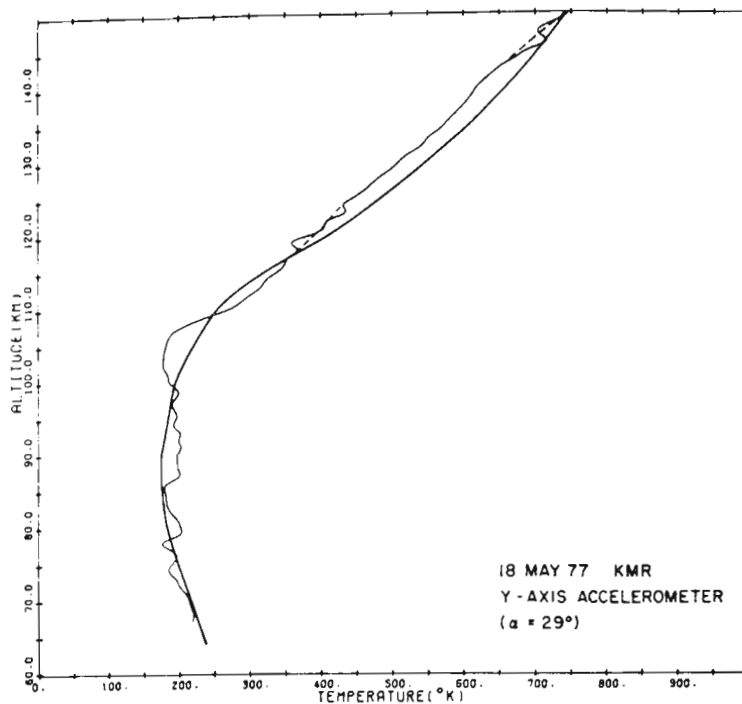Figure 17. The Temperature Profile Determined From the
Density Results Under the Assumption of Hydrostatic Equi-
librium With the Model Temperature Profile Shown for
Comparison

4. COMPARISONS

Since several different sensors and different analysis techniques were used to
make measurements during this period, several comparisons can be made. An
additional measurement of the drag acceleration on the AFGL sphere was obtained
from the ALCOR-Radar doppler velocity wide band data. The analysis of this data
was performed by Xonics, Inc. (Fletcher[15, 16]). The results of the radar data
analysis are shown in Figure 18 compared to the drag acceleration measurements
of the x- and y-axis accelerometers. Below 66 km and above 72 km, the measure-
ments are in good agreement. The error quoted for the analysis of the radar data
is ±3 percent, and the smoothing interval was chosen to be 10 k ft (~3 km).

15. Fletcher, E.T., Jr. (1977a) Private communication, Letter 25 July 1977
    from E.T. Fletcher, Jr., XONICS Corporation to C.R. Philbrick, AFGL.

16. Fletcher, E.T., Jr. (1977b) Private communication, Letter 7 November 1977
    from E.T. Fletcher, Jr., XONICS Corporation to Maj. Christian SAMSO/
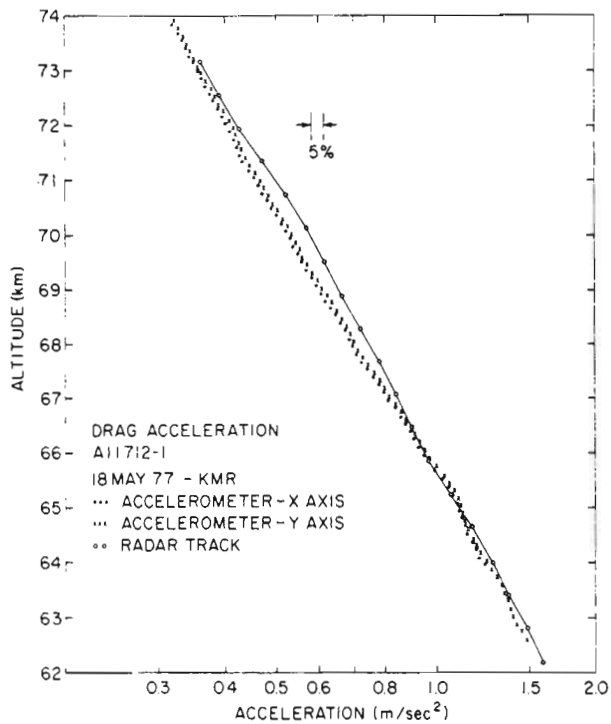   RSSP.

33

Figure 18. Measurements of the Drag Acceleration Measured by the X- and Y-axis Accelerometers Compared to the Sphere Draf Acceleration Determined From the ALCOR Radar Track (Fletcher[16])

The error bar on the relative profile for the accelerometer measurements is probably less than 3 percent. Thus, neither of the error bars of the two measurements quite overlaps the other set of data between 68 and 71 km. A possible consideration is that the large smoothing interval used on the radar data could introduce an error over the interval. The error associated with the radar tracking result may be considered to be a minimum measurable acceleration level, rather than a ±value over the entire measurement interval. From this point of view, the rather good agreement at low altitudes (62 to 67 km) is encouraging. The ALCOR Radar data is not available for this flight in the 80 km region, but if it were available the error bar on the result could be assigned with more confidence. If the results of an earlier flight on 31 August 1976 are considered, the minimum usable acceleration information from the radar track of the sphere in the 80 km regions was about 0.03 to 0.05 m/sec^2 depending on the degree of smoothing. If the radar level of performance was similar for this test, then the accuracy of the radar determined accelerations in the 70 km region may be as poor as 6 to 10 percent and thereby overlap the accelerometer measurements.

34

Figures 19, 20, and 21 show intercomparisons between the accelerometer measurements, rocketsonde measurements, and the No. 2029 Robin sphere, standard data program (Kennedy and Hackerson[2]) and the ALCOR-OPT 1 data reduction program (Fletcher[15, 16]). The standard data reduction program of the Robin data shows the same general trend as the ALCOR data between 60 and 90 km, but are less structured due to the large smoothing interval. The Robin data in the 45 to 60 km range have historically been known to differ systematically from the rocketsonde data. This difference has been attributed to a bias in the drag table or wind currents near the stratopause region and the data are not recommended for use below 60 km (Kennedy and Hackerson[2]).

The ALCOR-OPT 1 analysis of the Robin data (Fletcher[15]) shows much finer detail in the profile structure. In some regions the agreement with the accelerometer measurements is excellent, while in others poor; in fact, it's almost opposite in phase. The profiles were separated in time by about 20 min and in space by about 83 km. A wave system of 2nd order or higher would be required to produce the general features of both of these profiles in the 60 to 90 km region. The present knowledge of the density variability that may reasonably be expected from propagating gravity waves in the 70 to 90 km region is poor. Above 90 km, most of the structure observed in the Robin data is probably not real. Below 60 km, the Robin measurements from ALCOR data are somewhat closer to the rocketsonde than the standard reduction program results; however, the average difference is larger than would be expected from the assigned ±3 percent error (Fletcher[16]) on the Robin data and the spatial, temporal and instrumental RMS variability of rocketsonde data (Cole and Kantor,[1] also cf. Table 6).

Figure 22 shows the density ratio measurements for the AFGL sphere accelerometer, radar drag measurements (Fletcher[16]) and the rocketsonde measurements obtained 20 min later. The radar determined acceleration and density are listed in Table 7, where the results have been converted to metric units. These density ratios reflect the features shown in the acceleration results of Figure 18. The difference between the accelerometer measurements and the radar tracking data, may be due to a combination of a larger error in the radar results at higher altitudes and the effect of the smoothing interval used on the radar data. The difference between the rocketsonde and the radar track data at 57 km is about 8-1 2 percent. If the RMS error in the rocketsonde data, ~1.8 percent, is added to the expected RMS variability of the corresponding spatial, ~0.6 percent, and temporal, ~1.8 percent, differences (cf. Table 6 and Cole[17]), the observed difference is almost double this sum. Even through the radar determined acceleration

17. Cole, A. E. (1977) Private communication, Memorandum for the Record on Time and Space Variability of Density at Kwajalein.
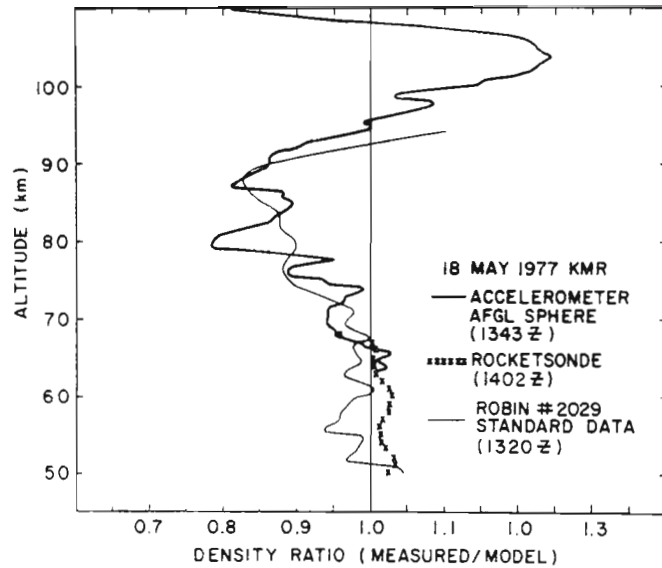
Figure 19. Comparison of the Accelerometer Measurements, Rocketsonde Measurements and the Results of the Standard Data Reduction of the Robin Sphere No. 2029 (Kennedy and Hackerson[2])
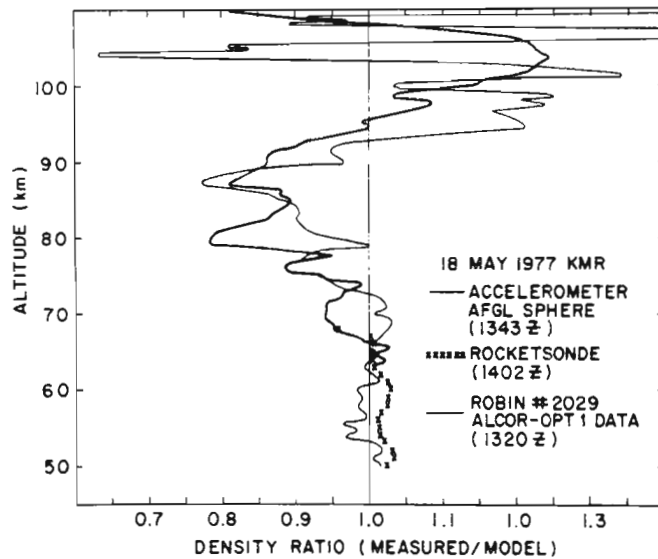

Figure 20. Comparison of the Accelerometer Measurements, Rocketsonde Measurements and the Results of the ALCOR-OPT 1 Data Reduction of the Robin Sphere No. 2029 (Fletcher[15])

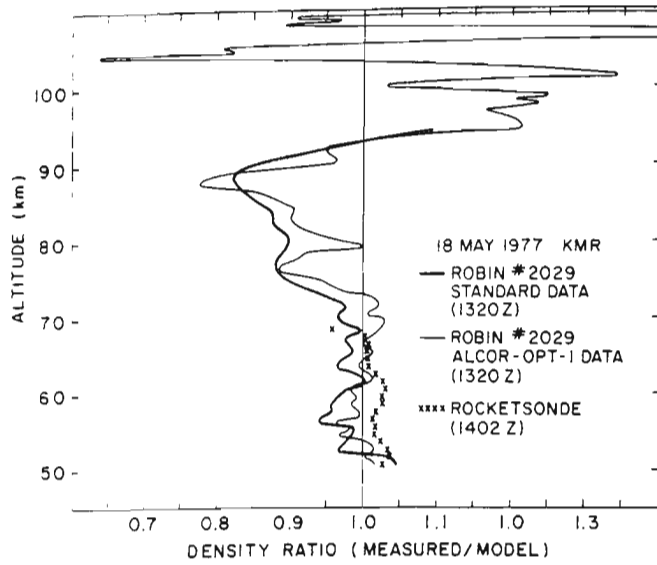Figure 21. Comparison of the Rocketsonde Measurements, the Results of the Standard Data Reduction (Kennedy and Hackerson[2]) and the Results of the ALCOR-OPT 1 Data Reduction (Fletcher[15]) for Robin Sphere No. 2029
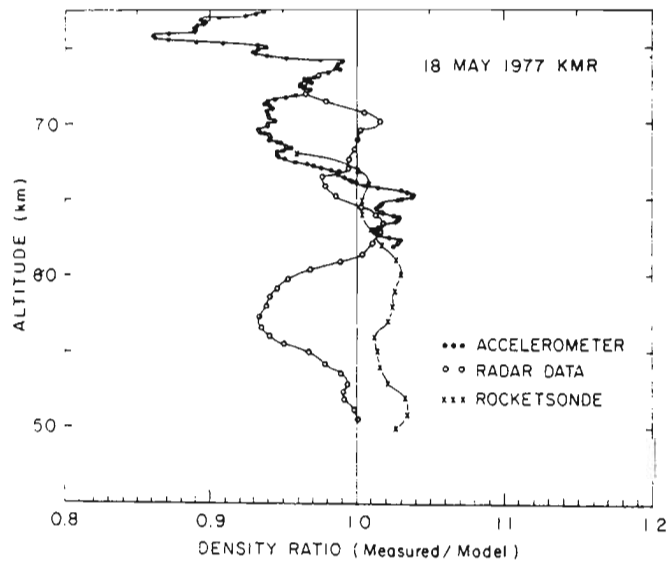

Figure 22. Comparison of the Measurements of the AFGL Accelerometer and the Determination Made From ALCOR Drag Acceleration Measurements on the AFGL Sphere (Fletcher[16]) Shown With the Rocketsonde Results

37

Table 7. Drag Acceleration and Density Data Derived From ALCOR Radar Track of AFGL Sphere, Converted to Metric Units From XONICS Analysis (Fletcher[15, 16])

T^+ (sec)	Altitude (km)	Density (kg/m^3)	Accelerometer (m/sec^2)	ρ/ρ Model
378.96	73.15	5.78^{-5}	0.360	.973
379.37	72.54	6.23^{-5}	0.390	.964
379.79	71.93	6.80^{-5}	0.426	.965
380.20	71.32	7.53^{-5}	0.469	.979
380.61	70.71	8.41^{-5}	0.520	1.005
381.02	70.10	9.22^{-5}	0.570	1.016
381.43	69.49	9.90^{-5}	0.614	1.002
381.84	68.88	1.08^{-4}	0.663	1.001
382.25	68.27	1.16^{-4}	0.719	.998
382.66	67.67	1.25^{-4}	0.780	.995
383.06	67.06	1.36^{-4}	0.838	.994
383.47	66.44	1.44^{-4}	0.897	.977
383.87	65.84	1.56^{-4}	0.969	.978
384.28	65.23	1.70^{-4}	1.059	.985
384.68	64.62	1.87^{-4}	1.157	1.003
385.08	64.01	2.04^{-4}	1.265	1.013
385.48	63.40	2.22^{-4}	1.373	1.018
385.88	62.79	2.38^{-4}	1.481	1.016
386.28	62.18	2.55^{-4}	1.589	1.011
386.68	61.57	2.73^{-4}	1.706	1.004
387.08	60.96	2.90^{-4}	1.814	.988
387.47	60.35	3.06^{-4}	1.922	.968
387.87	59.74	3.25^{-4}	2.040	.953
388.26	59.13	3.46^{-4}	2.177	.946
388.66	58.52	3.71^{-4}	2.334	.941
389.05	57.91	3.98^{-4}	2.511	.938
389.44	57.30	4.26^{-4}	2.687	.934
389.84	56.69	4.60^{-4}	2.893	.935
390.23	56.08	4.98^{-4}	3.138	.942
390.62	55.47	5.40^{-4}	3.143	.950
391.01	54.86	5.92^{-4}	3.717	.968

error shou
ments indi
Figur
Model (Co
to the nex
and is see
The conclu
measurem
The
by passiv
for the p
techniqu
the data
served d
A more
techniqu

Fig
are
Atm

18. Cole, A
     AFCR

error should be small at this altitude, the 2σ difference between these measurements indicates a difficulty for further study.

Figure 23 is added to show the relation between the newer Tropical Atmosphere Model (Cole and Kantor[18]) which will probably be adopted as part of the supplements to the new U.S. Standard Atmosphere. The model shown is for May at $0°$ latitude and is seen to agree with the measurements better than the older USSAS 1966 model. The conclusion is that where a model information is needed because of lack of measurements, then this model would be a better choice.

The improvements in capability for measurements of atmospheric properties by passive sphere tracking is evident in the data presented. The results presented for the piezoelectric accelerometer indicate the capabilities of this relatively new technique. These two advancements have increased the level of scrutiny to which the data can be reasonably subjected and thus indicate some differences. The observed differences dictate the direction for further study of this and other data sets. A more complete comparison of the results obtained by the various measurement techniques and details of the analysis of errors will be the subject of future reports.
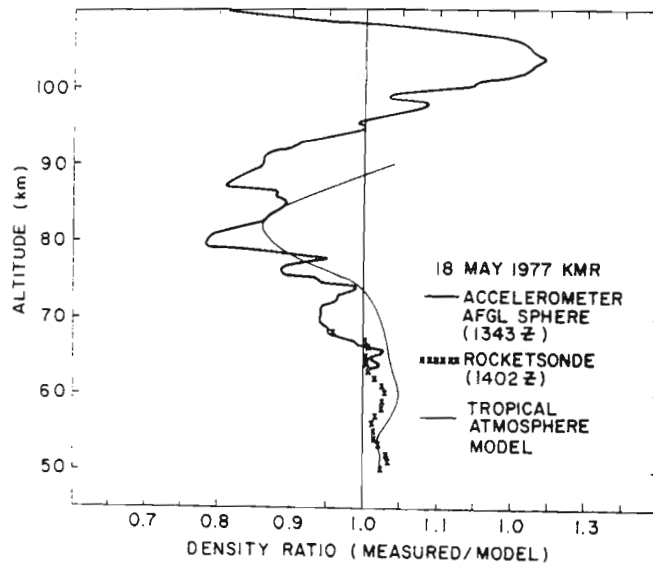

Figure 23. The Accelerometer Results and Rocketsonde Results are Shown With a Comparison to the Values of the Tropical Atmosphere Model for May at $0°$ Latitude (Cole and Kantor[18])

18. Cole, A.E., and Kantor, A.J. (1975) Tropical Atmosphere 0 to 90 km, AFCRL-TR-75-0527, AFGL, Hanscom AFB, Massachusetts.

References

1. Cole, A. E., and Kantor, A. J. (1977) Private communications.

2. Kennedy, B. W., and Hackerson, L. D. (1977) Analysis of Meteorological Data at Kwajalein Missile Range for WTR Mission 2333, ASL.

3. Martin, L., and Azzarelli, T. (1977) Wind and Density Measurements on Four ROBIN Spheres, XONICS DCD391.

4. Hanrahan, T. (1977) Evaluation of Doppler Modulation and Angle Error Effects on ROBIN Sphere Atmospheric Density Estimates, XONICS DCD426.

5. Bailey, A. B., and Hiatt, J. (1972) AIAA 10:1436.

6. Schaaf, S. A., and Chambre, P. L. (1958) Fundamentals of Gas Dynamics, 687.

7. Rose, M. H. (1964) Phys. Fluids I:1262.

8. Corbin, V. L. (1975) Private communication of unpublished study, Drag Coefficients from Free Molecular Flow to Continuum Flow for Mach Numbers 1.5 to 6.0.

9. USSAS (1966) U. S. Standard Atmospheric Supplements, 1966, U. S. Government Printing Office, Washington, D. C.

10. Salah, J. E. (1967) Kwajalein Standard Atmosphere, MIT Lincoln Laboratory Technical, Note 1967-14.

11. Thomson, W. T. (1948) Mechanical Vibrations.

12. VanName, F. W., Jr. (1958) Analytical Mechanics.

13. List, R. J. (1968) Smithsonian Meteorological Table, 6th Edition, Smithsonian Institution, Washington, D. C.

14. Philbrick, C. R. (1977) Private communication, Letter Report of Preliminary Data for TDV-1 on 18 May 1977, dated 29 June 1977 from C. R. Philbrick, AFGL, to Capt. Bose, SAMSO/RSSR.

15. Fletcher, E. T., Jr. (1977a) Private communication, Letter 25 July 1977 from E. T. Fletcher, Jr., XONICS corporation to C. R. Philbrick, AFGL.

16. Fletcher, E.T., Jr. (1977b) Private communication, Letter 7 November 1977 from E.T. Fletcher, Jr., XONICS Corporation to Maj. Christian SAMSO/RSSP.

17. Cole, A.E. (1977) Private communication, Memorandum for the Record on Time and Space Variability of Density at Kwajalein.

18. Cole, A.E., and Kantor, A.J. (1975) Tropical Atmosphere 0 to 90 km, AFCRL-TR-75-0527, AFGL, Hanscom AFB, Massachusetts.